Catal Lett (2008) 126:125–133
DOI 10.1007/s10562-008-9591-5

# Surfactant-Controlled and Microwave-Assisted Synthesis of Highly Active $Ce_xZr_{1-x}O_2$ Nano-Oxides for CO Oxidation

**Benjaram M. Reddy · Pankaj Bharali · Yeong-Hui Seo · Eko Adi Prasetyanto · Sang-Eon Park**

Received: 10 June 2008 / Accepted: 11 July 2008 / Published online: 2 August 2008


**Abstract** Uniform nanosized, mesoporous and high specific surface area ceria–zirconia (1:1 mole ratio) solid solutions were synthesized employing a poly-block copolymer surfactant combined with microwave or thermal treatment. For comparison purpose an identical composition $Ce_xZr_{1-x}O_2$ mixed oxide was also prepared by a conventional coprecipitation method. The surface and bulk structure of the synthesized samples were investigated using X-ray diffraction (XRD), small angle X-ray scattering (SAXS), Raman spectroscopy, scanning electron microscopy (SEM), transmission electron microscopy (TEM), BET surface area and BJH pore size distribution (PSD) methods. The catalytic activity was evaluated for CO oxidation at normal atmospheric pressure. The $Ce_xZr_{1-x}O_2$ solid solutions obtained through surfactant use exhibited high specific surface area and mesoporosity. The XRD measurements revealed the presence of cubic $Ce_{0.75}Zr_{0.25}O_2$ and $Ce_{0.6}Zr_{0.4}O_2$ phases in the case of conventional coprecipitation and surfactant controlled synthesized samples, respectively. The Raman measurements revealed existence of more oxygen defects in the surfactant-controlled and microwave treated sample. The SEM images suggested that all samples consist of typical spherical agglomerates with almost uniform size within the nanometer size range. The TEM measurements revealed nanosized crystallites in a narrow range between 4 and 8 nm, and densely packed in the case of conventional precipitation and microwave treated samples. Interestingly, the $Ce_xZr_{1-x}O_2$ solid solution obtained by surfactant-controlled method and treated with microwave radiation exhibited better CO oxidation activity than other samples. Enhanced activity of surfactant-controlled and microwave treated sample is correlated with its unique physicochemical characteristics.

**Keywords** Ceria–zirconia · Nano-oxides · Surfactant-controlled · Microwave-assisted · Catalyst characterization · CO oxidation

B. M. Reddy (✉) · Y.-H. Seo · E. A. Prasetyanto · S.-E. Park (✉)
Laboratory of Nano-Green Catalysis, Department of Chemistry, Inha University, Incheon 402-751, Republic of Korea
e-mail: mreddyb@yahoo.com

S.-E. Park
e-mail: separk@inha.ac.kr

B. M. Reddy · P. Bharali
Inorganic and Physical Chemistry Division, Indian Institute of Chemical Technology, Uppal Road, Hyderabad 500607, India

## 1 Introduction

Ceria ($CeO_2$) has been recognized as one of the most important rare-earth oxides in view of its numerous applications. In conjunction with the advantages of nanotechnology it is finding many applications in the fields of catalysis, sensor technology, and biomedical sciences [1–10]. The use of pure $CeO_2$ is generally discouraged as it undergoes rapid sintering at high temperatures, thereby loosing its crucial oxygen storage/release capacity (OSC) characteristics. Therefore, several investigations were focused on the application of $Ce_xZr_{1-x}O_2$ solid solutions instead of $CeO_2$ alone [4, 5, 7, 9]. In the mixed oxides of ceria–zirconia, $Zr^{4+}$ cation partially substitutes for $Ce^{4+}$ in the lattice of $CeO_2$, forming a solid solution. Compared to pure $CeO_2$, the $Ce_xZr_{1-x}O_2$ solid solutions can maintain the reversible $Ce^{3+}/Ce^{4+}$ redox property even after exposure to harsh reaction conditions and exhibit improved thermal resistance and better catalytic activity [7]. Therefore, $Ce_xZr_{1-x}O_2$ composite oxides are the key materials for

numerous practical applications in catalysis [3, 4, 7], such as three-way catalytic converters (TWC) for automotive exhaust depollution [4, 5], in water-gas shift catalysis for production and purification of hydrogen [7], and solid electrolytes for solid-oxide fuel cells [11] and so on. In view of their huge commercial significance several preparative routes were employed to make them which include coprecipitation [12], impregnation [13], sol–gel [14], mechanical milling [15], spray pyrolysis [16], sputtering [17], chemical vapor deposition [18] and other methods. It is a well-known fact that synthetic methodology and process conditions strongly influence the physicochemical characteristics such as specific surface area, phase composition, crystallite size, redox ability, and OSC of the resulting ceria–zirconia mixed oxides [3, 5, 7]. For example, the traditional preparation methods based on sol–gel and related routes require expensive precursors, such as alkoxides. Also the atomic homogeneity of the materials obtained through some of these routes is rather poor although they exhibit controlled textural and surface properties [19]. Therefore, several attempts are underway to develop an efficient and cost effective preparative methodology to obtain uniform and catalytically active $Ce_xZr_{1-x}O_2$ nano-oxides for various applications.

There is a growing interest in microwave processing of materials over conventional methods because of significant reduction in manufacturing cost, in terms of energy and time, better product homogeneity, and unique microstructures resulting in better physicochemical characteristics [20–22]. The theory of microwave heating and the interaction of materials with the microwaves have been elaborated in several publications in recent times [23, 24]. As known the microwave heating is fundamentally different from the conventional heating wherein the heat generates internally through material-microwave interaction instead of originating from an external heating source [25]. Regardless of the relatively large body of published work on this topic, the exact reason why microwave irradiation is able to enhance chemical processes is still unknown. Of course, the existence of so-called 'specific microwave effects' which cannot be duplicated by conventional heating and result from the uniqueness of the microwave dielectric heating phenomenon is largely undisputed [26].

The use of surfactant-assisted routes has gained lot of attention recently for the synthesis of controllable nanoparticle dispersions with high specific surface area and defined porosity. In the present work, a surfactant-assisted synthesis method is applied to prepare ceria–zirconia solid solutions, to obtain high surface area materials and to further study the features of their crystalline structure and how these factors affect their catalytic activity. Another objective of the present investigation was to explore the usefulness of the microwave to synthesize homogeneous $Ce_xZr_{1-x}O_2$ solid solutions. For the purpose of better comparison, an identical molar composition ceria–zirconia solid solution was also prepared by a conventional coprecipitation method. A multitechnique characterization by X-ray diffraction (XRD), small angle X-ray scattering (SAXS), Raman spectroscopy (RS), scanning electron microscopy (SEM), transmission electron microscopy (TEM) and $N_2$ adsorption was performed to uncover the structural and textural properties of the synthesized samples. Finally, the catalytic activity of the synthesized composite oxides was evaluated for CO oxidation at normal atmospheric pressure.

## 2 Experimental

### 2.1 Catalyst Synthesis

A micellar solution (~5%) of Pluronic F-127 (Sigma, USA) was prepared by dissolving in distilled water at ambient temperature under vigorous stirring for 3 h and an appropriate amount of aqueous ammonia was added. The desired quantities of cerium(III) nitrate and zirconium(IV) nitrate (1:1 mole ratio based on oxides) precursors were dissolved separately in deionized water and mixed together. The resulting clear solution of the metal salts was added drop-wise to the surfactant solution under continuous stirring for 5 h. The obtained reddish brown precipitate was divided into two equal portions and transferred into Teflon autoclaves. A portion of it was subjected to microwave irradiation (Sample Code MW) at 373 K for 2 h under static conditions with an operating power of 300 W (100%). Another portion was subjected to conventional thermal heating (Sample Code TM) at 373 K for 24 h. The solid products were then filtered off, washed with copious amounts of deionized water and dried at 393 K for 24 h and calcined at 823 K for 6 h in air atmosphere. For comparison purpose an identical composition Ce–Zr-oxide from the same precursors was prepared by a co-precipitation method (Sample Code PT). The desired quantities of precursors were dissolved separately in distilled water and mixed together under mild stirring condition. To this clear mixture solution, dilute ammonium hydroxide was added drop-wise to precipitate the mixed-metal hydroxide gel (pH 8). The resulting slurry was filtered off and thoroughly washed with deionized water, dried at 393 K for 12 h and calcined at 823 K for 6 h in air atmosphere.

### 2.2 Structural Characterization

X-ray powder diffraction patterns were acquired with a Rigaku Multiflex instrument using nickel-filtered Cu Kα

(0.15418 nm) radiation source and a scintillation counter detector. Crystalline phases were identified by matching the experimental patterns with the PDF-ICDD files. The mean particle size of the crystalline oxide phases was estimated with the help of Scherrer equation using the XRD data of all prominent lines. The lattice parameter 'a' was calculated by a standard cubic indexation method using the intensity of the most prominent peak (111). The small-angle X-ray scattering experiments were performed at the 4C1 Beamline of the Pohang Accelerator Laboratory, Korea using an X-ray source $\lambda = 0.1608$ nm. Measurements were made using a two-dimensional charge-coupled detector (2D CCD) (Roper Scientific, Trenton, NJ). The Raman spectra were recorded with a LabRam HR800UV Raman spectrometer (Horiba Jobin-Yvon) equipped with a confocal microscope and liquid-nitrogen cooled CCD detector. The emission line at 325 nm from He–Cd laser (Melles Griot Laser) was focused on the sample under the microscope, with the diameter of the analyzed spot being $\sim$1 μm. The time of acquisition was adjusted according to the intensity of Raman scattering. The wave number values reported from the spectra are accurate to within 1 $cm^{-1}$. In order to ascertain the homogeneity of the sample, spectra were recorded at various points and compared. All samples synthesized in this study were found to be highly homogeneous. The SEM images were collected with a JEOL 630-F microscope. Before measurements, samples were dispersed on a steel plate surface and coated with Pt metal. The TEM images were obtained on a JEM-2010 (JEOL) instrument equipped with a slow-scan CCD camera and at an accelerating voltage of 200 kV. Samples were sonically dispersed in ethanol and deposited on a carbon coated copper grid before examination. The BET surface area and BJH pore size distribution measurements were made by $N_2$ adsorption/desorption at liquid-nitrogen temperature using a Micromeritics ASAP 2020 instrument. Before analysis, samples were evacuated for 3–4 h at 523 K in the degassing port of the instrument.

### 2.3 Catalytic Activity

The catalytic activity of the calcined nano-oxides was evaluated for oxidation of CO in a fixed bed micro-reactor at normal atmospheric pressure. For each run, $\sim$0.1 g of fine powders of the sample diluted with fine quartz particles of the same sieve fraction was used. Temperature was measured directly at the catalyst bed, using a thermocouple placed in the hollow shaft of the reactor. High purity gases and gas mixtures namely, argon (purity, >99.999%), 9.98% CO in argon (CO purity, >99.997%) and 10.2% $O_2$ in argon ($O_2$ purity, >99.995%) were used (Air Liquide) directly without further purification. The gas flow rates were maintained by mass flow controllers. The CO and $CO_2$ gas concentrations were measured with an Uras 14 infrared analyzer module, and the $O_2$ concentration was measured with a Magnos 16 analyzer (Hartmann & Braun). Prior to oxidation of CO, the catalyst was heated to 773 K in 10.2% $O_2$/Ar gas mixture, with a heating ramp of 10 K $min^{-1}$, and kept at the final temperature for 1 h. The oxidized sample was then purged in argon and cooled to the desired starting reaction temperature. The $CO/O_2$ reactant feed ratio was 1, and the partial pressures of CO and $O_2$ were in the range of 10 mbar.

## 3 Results and Discussion

Textural analyses of the conventional precipitation sample and the surfactant assisted synthesized samples revealed some differences in the shapes of the $N_2$ adsorption–desorption isotherms (Fig. 1). The shapes of the hysteresis loops are almost same (type IV) for the surfactant assisted and microwave (MW) or thermally (TM) treated samples. However, the conventional precipitation (PT) sample exhibited a different isotherm. This behaviour is associated with a shift of the mesoporous size towards a lower range. The MW and TW samples exhibited a high specific surface area and pore volume than the conventional PT sample (Table 1). In fact, the as synthesized samples subjected to thermal treatment at 393 K exhibited much higher specific surface areas (200–250 $m^2g^{-1}$). As known, in the case of conventional coprecipitation method, during the precipitation stage, water molecules normally fill the internal pores to form hydrous metal oxides. When these hydrous solids are dried, the capillary pressure at the liquid-vapour interface in the pores produces stress on the metal oxide

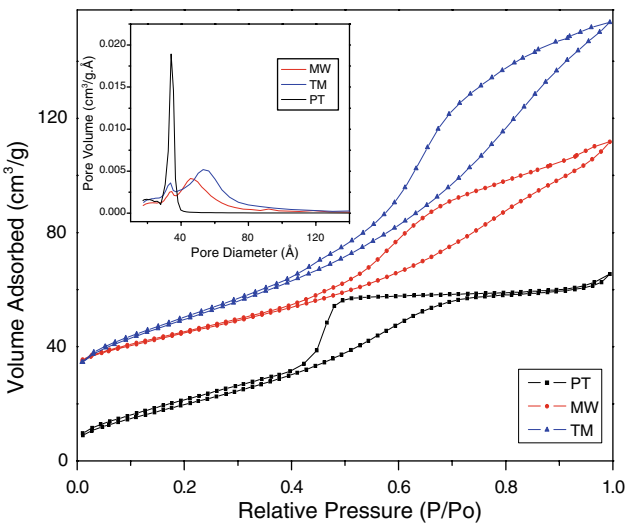


**Fig. 1** $N_2$ adsorption–desorption isotherms and BJH pore size distribution of $Ce_xZr_{1-x}O_2$ nano-oxides synthesized by surfactant-controlled and microwave (MW) or thermal treatment (TM) and conventional precipitation (PT) methods

**Table 1** BET surface area, pore volume, crystallite size, and cell 'a' parameter measurements of $Ce_xZr_{1-x}O_2$ nano-oxides synthesized by surfactant-controlled and microwave (MW) or thermal treatment (TM) and conventional precipitation (PT) methods

| Sample | Surface area ($m^2\ g^{-1}$) | Pore volume ($cm^3\ g^{-1}$) | Crystallite size (nm) | Cell 'a' parameter (Å) |
|---|---|---|---|---|
| MW | 122.9 | 0.1455 | 4.6 | 5.317 |
| TM | 143.6 | 0.2224 | 4.9 | 5.326 |
| PT | 95.9 | 0.1030 | 5.5 | 5.395 |

framework, thus provoking the collapse of the pore network, and in turn, reduces their specific surface area. However, in the case of surfactant-controlled method, the presence of surfactant leads to interactions between the deprotonated hydroxyl groups and the positively charged surfactant head groups, which may incorporate into the M–O–M framework, thus forming a polymeric network of hydrous oxides such as $nMO_x(O\text{-Surfactant})_y \cdot mH_2O$ [27]. The capillary pressure in the pores is generally proportional to the surface tension and the added surfactant can reduce water surface tension in the pores. Which in turn decreases the dried gel shrinkage degree, therefore, a high specific surface area is normally achieved by adopting surfactant-controlled method.

The crystalline structures of the synthesized solids were investigated by X-ray powder diffraction analysis. Figure 2 shows the XRD patterns of the samples calcined at 823 K and the corresponding crystallite size and cell 'a' parameter values are presented in Table 1. Only the broad diffraction lines due to cubic fluorite type phase with the composition $Ce_{0.75}Zr_{0.25}O_2$ (PDF-ICDD 28-0271) are identified in the case of PT sample. In the case of surfactant-controlled synthesized samples, the intensity of the XRD lines is relatively broader due to smaller crystallite size. Also a slight shift in the peak positions towards higher two-theta values is noted which indicate that along with the formation of smaller crystallites some compositional changes are also taking place. A detailed analysis of the XRD patterns established the formation of $Ce_{0.6}Zr_{0.4}O_2$ phase (PDF-ICDD 38-1439) in the case of surfactant-controlled synthesized samples [28, 29]. The shift in the peak positions towards higher two-theta values is primarily due to an increase of zirconium content in the ceria unit cell, since the ionic radius of $Zr^{4+}$ (0.84 Å) is smaller than $Ce^{4+}$ (0.97 Å) [7, 29]. The corresponding crystallite size and cell 'a' parameter values, elaborated in the proceeding paragraph, also support this phenomenon. As reported by Kenevey et al. [30] the composition change is mainly due to phase segregation phenomenon, which is considered to be surface energy driven. Solid solutions are normally stable as long as the crystallite size does not exceed a critical size, above which the surface energy contribution to the total energy of the system becomes too small to allow its stabilization thereby leading to the phase segregation [30]. An important observation to be mentioned from XRD results is that, within the detection limits of the XRD technique, there is no evidence about the presence of t-$ZrO_2$ or m-$ZrO_2$ phases in any of the samples investigated in this study. Most importantly, the $Ce_xZr_{1-x}O_2$ mixed oxides obtained through the present method exhibited only single phase with cubic structure, confirming that Ce- and Zr-ions are uniformly distributed in the structure and formed a homogeneous solid solution. Of course, the XRD patterns of the samples are relatively broad due to nano-sized nature of the crystallites formed.

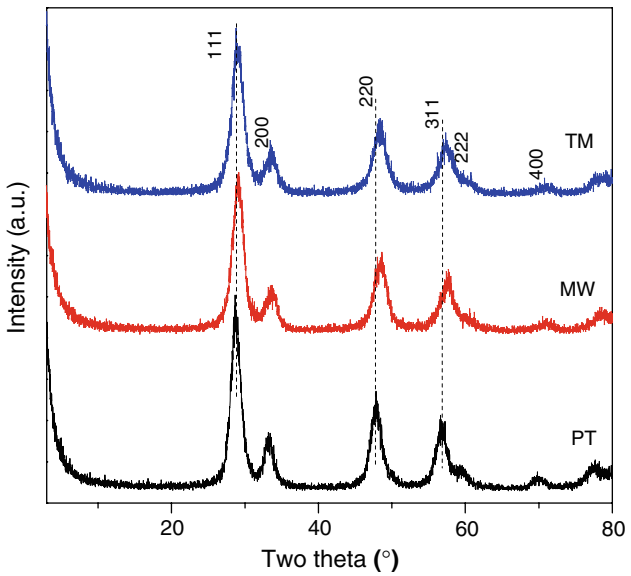


**Fig. 2** X-ray powder diffractions of $Ce_xZr_{1-x}O_2$ nano-oxides synthesized by surfactant-controlled and microwave (MW) or thermal treatment (TM) and conventional precipitation (PT) methods

The average crystallite size ($D_{XRD}$) of $Ce_xZr_{1-x}O_2$ in various samples is presented in Table 1. In comparison to a pure ceria prepared by an identical precipitation method, which had a crystalline size of 10.3 nm [31], the $Ce_xZr_{1-x}O_2$ solid solutions exhibited much smaller crystallite sizes. Therefore, it can be stated from the present study that zirconium addition to ceria effectively inhibits the crystallite growth. As established in the literature, the formation of solid solutions between ceria and zirconia retards the crystallite growth and facilitates the formation of thermodynamically more stable phases as noted in the present study [32].

Lattice parameter estimations provide useful information on the location of foreign cations in the ceria lattice. In particular, whether the foreign cations entered into the lattice resulting in the formation of a solid solution or remained as a separate phase demarcated by a phase boundary. Using the most intense (111) line of the $Ce_xZr_{1-x}O_2$ XRD patterns, cubic indexation and calculation of the unit cell parameter was carried out and presented in Table 1 [33, 34]. As can be observed from Table 1, there is a decrease in the cell 'a' parameter of $Ce_xZr_{1-x}O_2$ solid solutions, in comparison to pure $CeO_2$ (5.412 Å), which again is dependent on the preparation methodology [31]. Interestingly, the decrease is slightly more in the case of microwave treated sample when compared to that of other samples. As known, the decrease in the cell 'a' parameter is due to shrinkage of the lattice when $Ce^{4+}$ (0.97 Å) ions are replaced with smaller cations of $Zr^{4+}$ (0.84 Å), in agreement with Vegard's law [35, 36]. The decrease in the cell 'a' parameter values is an evidence for incremental enrichment of Zr-content in the Ce unit cell [37, 38]. According to literature, the Zr–O bond length in the cubic $ZrO_2$ is 2.21 Å, which is much shorter than the Ce–O bond length of 2.36 Å in cubic $CeO_2$ [39]. Therefore, when zirconium substitutes for cerium centers in cubic fluorite lattice, shrinkage of the lattice takes place due to nonequivalent metal–oxygen bond lengths and different bonding positions [39]. As per the literature, the SAXS technique allows obtaining structural information about inhomogeneities of the electron density in the samples, with a characteristic length on the order of tens to hundred of Å [40]. It is also known as an appropriate technique to obtain information on the size and shape of the particles. A qualitative examination of the samples synthesized in this study revealed (Fig. 3) that there is a significant difference between the samples obtained by conventional coprecipitation method and the surfactant assisted method. However, there was no apparent difference in between the microwave and conventional thermal treatment samples. Of course, the SAXS patterns of all samples are typical of "Porodian" solids in agreement with their specific surface area and pore size distribution measurements [41].

As known, the cation order–disorder and lattice distortion could be easily detected by conventional X-ray diffraction method. However, the XRD technique does not allow accurate identification of distortions of oxygen sublattice and defects in the structure due to poor sensitivity of the technique to the oxygen atoms in the presence of heavy atoms such as Ce and Zr. Mobility of oxygen atoms in the lattice is most critical for most of the applications of ceria-based materials, both as ionic/electronic conductors and redox catalysts. Therefore, a deep insight into the structural features is highly desirable. Of course, Raman spectroscopy is an established technique sensitive to both M–O bond arrangement and lattice defects. The tetragonal phase ($P4_2/nmc$ space group) normally exhibits six Raman-active modes, while the cubic phase ($Fm3m$ space group) only presents one ($F_{2g}$) Raman-active mode [42, 43]. However, when the crystal symmetry is lower, more Raman modes are usually allowed. The Raman spectra of variously synthesized samples in this study are shown in Fig. 4. As presented in this figure, the Raman spectra of various samples show prominent broad peaks at ~460 and 620–640 $cm^{-1}$ and a weak band at ~330 $cm^{-1}$. The band at ~460 $cm^{-1}$ corresponds to the triply degenerate $F_{2g}$ mode and can be viewed as a symmetric breathing mode of oxygen atoms around cerium ions [42–45]. Generally, a

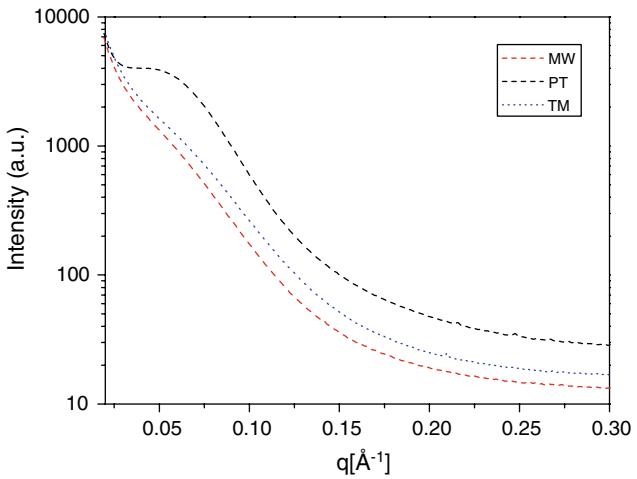


**Fig. 3** SAXS of $Ce_xZr_{1-x}O_2$ nano-oxides synthesized by surfactant-controlled and microwave (MW) or thermal treatment (TM) and conventional precipitation (PT) methods

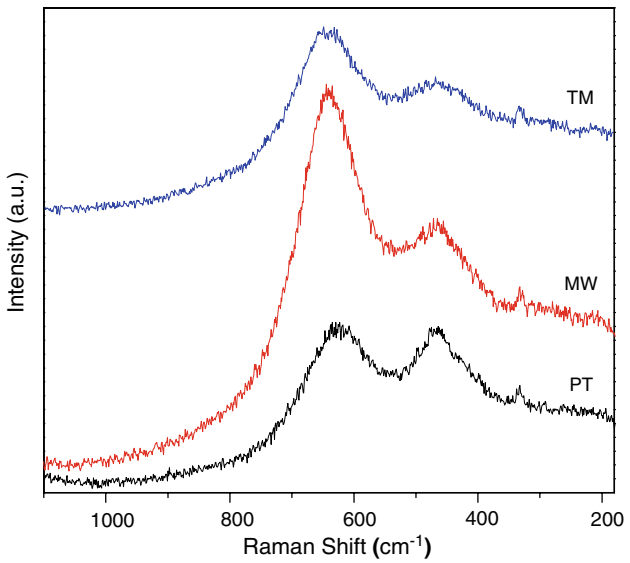


**Fig. 4** Raman spectra of $Ce_xZr_{1-x}O_2$ nano-oxides synthesized by surfactant-controlled and microwave (MW) or thermal treatment (TM) and conventional precipitation (PT) methods

strong 460 $cm^{-1}$ band with a weak ~320 $cm^{-1}$ peak indicates the presence of cubic phase, which is present in all samples. Interestingly, the typical characteristic band at ~460 $cm^{-1}$ in the case of PT sample is more intense when compared to that of other samples. It is a known fact in the literature that intensity of Raman band depends on several factors including grain size and morphology. In general, inhomogeneous strain and phonon confinement are responsible for broad and asymmetric character of the bands due to smaller particle sizes [46]. The Raman band in the 600–640 $cm^{-1}$ region has most often been attributed to defects [46, 47], and oxygen displacements that distort the cubic structure, breaking the cubic symmetry and selection rules of the cubic space group [7, 46]. Most importantly, this band is very strong in the case of MW sample and relatively weak in the case of PT sample. This could be one of the reasons for MW sample to exhibit better catalytic activity for CO oxidation described in the later paragraphs of this section.

The external morphologies of the samples were examined by SEM technique and the representative images are shown in Fig. 5. The SEM images reveal that all samples consist of typical spherical agglomerates with almost uniform size within the nanometer size range. In particular, all samples exhibited good homogeneity irrespective of the preparation method. Interestingly, the MW sample exhibited more amorphous features and densely packed agglomerates of smaller crystallites. The PT sample showed relatively better crystalline features followed by TM sample in line with XRD results. Interestingly, the method of preparation of $Ce_xZr_{1-x}O_2$ solid solutions did not reveal any significant change in the external morphology of the samples. To explore the structural features at atomic level, high-resolution TEM studies were also performed. The representative TEM images are shown in Fig. 6. The crystallite size in all samples is distributed in a narrow range between 4 and 8 nm, revealing that the ceria–zirconia crystallites of all the samples are highly homogeneous. The average crystallite size is about 6 nm observed by TEM, which is in good agreement with the values obtained from XRD analysis. Further, the high-resolution image contrasts obtained from the experimental images are found to be associated with the face centered cubic structure (fluorite) of the Ce–Zr-oxide [48]. Interestingly, the TEM images revealed that nano-oxides of $Ce_xZr_{1-x}O_2$ obtained by microwave treatment are randomly oriented and densely packed when compared to that of thermally treated sample (TM).

The catalytic activity of the $Ce_xZr_{1-x}O_2$ solid solutions obtained by different methods was investigated for CO oxidation. The conversion of CO as a function of reaction temperature is presented in Fig. 7. The catalytic activity measurements were performed at normal atmospheric pressure and the conversion of CO was evaluated as per the procedure described in our earlier publication [49]. The CO oxidation was observed to start after the temperature reached ~450 K in all cases and subsequently increased rapidly. The MW catalyst exhibited relatively better performance compared to that of other samples. The temperature at which 50% conversion occurred (light-off temperature) was found to be 554, 561, and 574 K for MW,

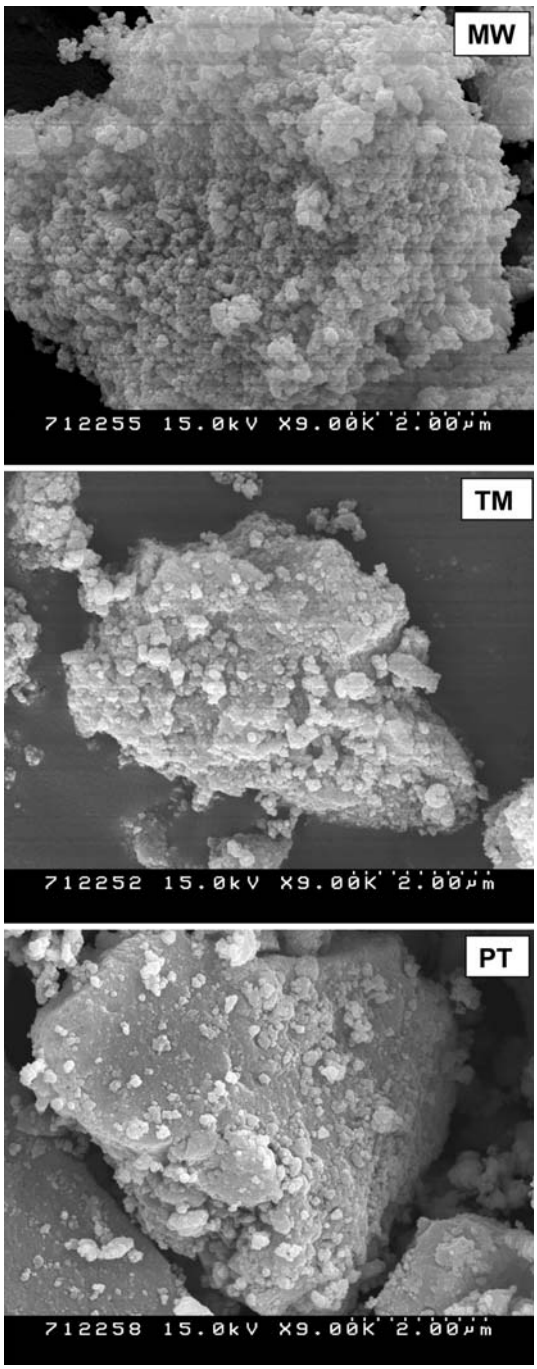


**Fig. 5** SEM micrographs of $Ce_xZr_{1-x}O_2$ nano-oxides synthesized by surfactant-controlled and microwave (MW) or thermal treatment (TM) and conventional precipitation (PT) methods

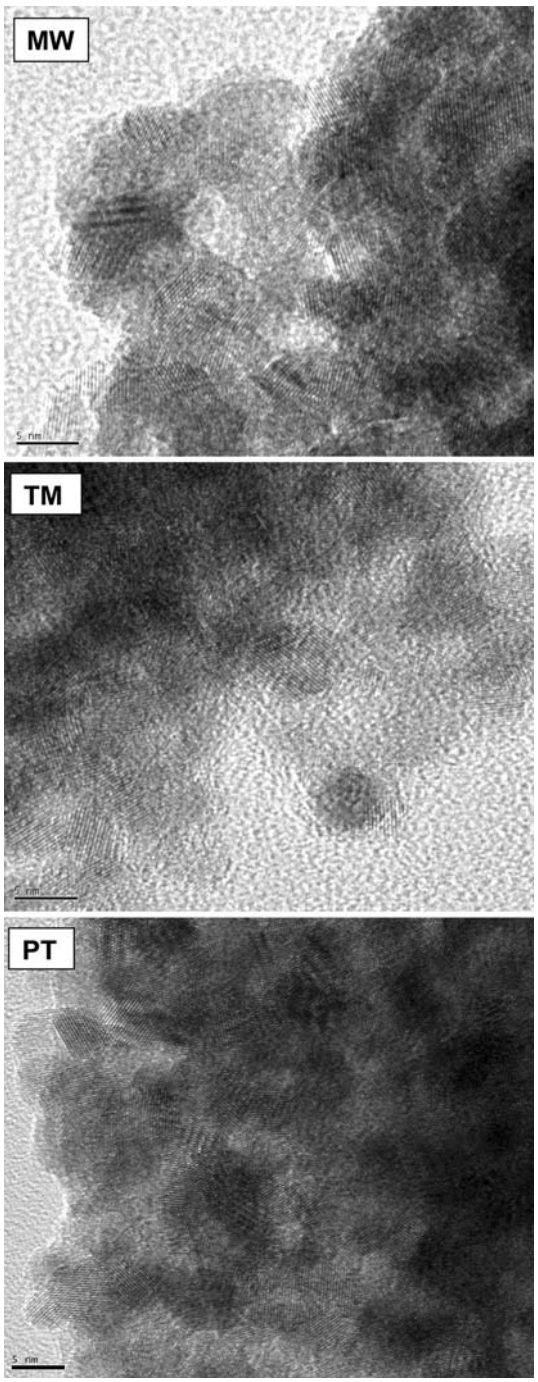


**Fig. 6** TEM micrographs of $Ce_xZr_{1-x}O_2$ nano-oxides synthesized by surfactant-controlled and microwave (MW) or thermal treatment (TM) and conventional precipitation (PT) methods

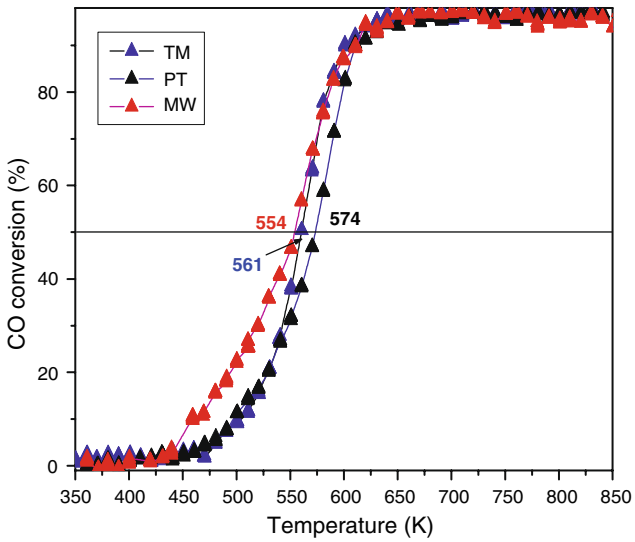


**Fig. 7** CO oxidation activity of $Ce_xZr_{1-x}O_2$ nano-oxides synthesized by surfactant-controlled and microwave (MW) or thermal treatment (TM) and conventional precipitation (PT) methods at normal atmospheric pressure

TM, and TP samples, respectively, giving rise to the catalytic efficiency order of MW > TM > PT. In all cases there was no big difference in the composition of the Ce–Zr-oxide solid solutions except their specific surface area. Interestingly, the reactivity order does not correlate with the specific surface areas of the samples. From the activity results it appears that the catalytic performance of $Ce_xZr_{1-x}O_2$ is certainly influenced by microwave treatment. It is worth mentioning here that both MW and TM samples exhibited similar crystallite sizes in the nano-range and TM sample showed more specific surface area than that of MW sample. Therefore, the catalytic performance is solely due to $Ce_xZr_{1-x}O_2$, which is influenced by the presence of oxygen vacancies and lattice defects. Ceria crystallizes in a cubic fluorite structure, where each cerium cation is coordinated by eight equivalent nearest-neighbor oxygen anions at the corners of a cube. The $Zr^{4+}$ insertion into the Ce core structure leads to the formation of defects in the ceria–zirconia lattice that induces a distortion of the oxygen sub-lattice. If the ceria–zirconia solid solution contains much less zirconium, it cannot induce sufficient stress, and the oxygen mobility within the bulk will not increase substantially. On the other hand, if the zirconium content is too high, it will reduce the quantity of the redox element Ce. Therefore, a definite balance between structural defects and the composition are the essential requirement, and a balance between these two parameters is a key factor to determine the CO oxidation activity of the $Ce_xZr_{1-x}O_2$ composite oxides [15]. Raman results provided strong evidence for the presence of more defects in the case of MW sample. Of course, further studies are essential to understand the positive influence of microwave irradiation on the defect formation and subsequent high catalytic activity of the sample.

Concerning the crystalline structure of ceria derived from supramolecular templates and how it affects the formation of lattice vacancies in the ceria structure and its catalytic properties, some questions still remain. It should be pointed out here that, in the structure containing cation

defects, the lattice oxygen ions around cationic defects are not fully bounced; these oxygen ions are mobile and more active than the normal ones under the reaction conditions because they may easily form free-like oxygen species by breaking M–O bond symmetry when additional energy is supplied. Therefore, the formation of cationic defects seems favouring free-like oxygen species generation in the bulk of the crystals that might migrate from the bulk to the surface, promoting the surface reaction. The present results indicate that cationic defect formation in the bulk structure may be a possible origin of high mobility of the lattice oxygen ions in ceria–zirconia solid solutions which eventually leads to more activity of this mixed oxide [7]. Further studies are highly essential to resolve some of these issues. Nevertheless, the application of microwave energy in the synthetic methodology of ceria–ziconia nano-oxides exhibits a positive influence on their catalytic activity for CO oxidation.

## 4 Conclusions

Synthesis of nanosized, uniformly distributed, mesoporous and high specific surface area ceria–zirconia solid solutions have been achieved via a neutral carbon block copolymer surfactant-controlled synthesis combined with microwave or thermal treatment. The surface and bulk properties of the synthesized samples were examined by using various techniques namely, XRD, SAXS, Raman spectroscopy, SEM, TEM, surface area, and pore size distribution methods. The catalytic activity for CO oxidation was evaluated at normal atmospheric pressure. The $Ce_xZr_{1-x}O_2$ nano-oxides synthesized by employing surfactant exhibited a high specific surface area and mesoporosity. XRD results confirmed the formation of cubic $Ce_{0.6}Zr_{0.4}O_2$ phase. Raman results revealed the existence of more oxygen defects in the surfactant-controlled and microwave treated sample. The SEM and TEM images suggested typical spherical agglomerates with uniform nanosized crystallites in the 4–8 nm size range. The $Ce_xZr_{1-x}O_2$ mixed oxide synthesized by surfactant-controlled method followed by microwave treatment exhibited better CO oxidation activity.

**Acknowledgments** This work was supported by Korea Science and Engineering Foundation (KOSEF) grant founded by the Korea Government (MOST) (NRL No. 36379-1). BMR thanks the Korea Federation of Science and Technology (KOFST), Republic of Korea for a visiting fellowship under the Brain Pool program.

## References

1. Park SD, Vohs JM, Gorte RJ (2000) Nature 404:265
2. Fu Q, Saltsburg H, Flytzani-Stephanopoulos M (2003) Science 301:935
3. Bernal S, Kaspar J, Trovarelli A (eds) (1999) Recent progress in catalysis by ceria and related compound. Catal Today 50:173
4. Trovarelli A (2002) In: Hutchings GJ (ed) Catalysis by ceria and related materials, catalytic science series, vol 2. Imperial College Press, London
5. Sugiura M (2003) Catal Surv Asia 7:77
6. Garcia MF, Arias AM, Hanson JC, Rodriguez JA (2004) Chem Rev 104:4063
7. Monte RD, Kaspar J (2005) J Mater Chem 15:633
8. Tarnuzzer RW, Colon J, Patil S, Seal S (2005) Nano Lett 5:2573
9. Reddy BM (2006) In: Fierro JLG (ed) Metal oxides: chemistry and applications, chapter 8. Marcel Dekker, New York, p 215
10. Andersson DA, Smiak SI, Skorodumova NV, Abrikosov IV, Johnsson B (2006) PNAS 103:3518
11. Jurado JR (2001) J Mater Sci 36:1133
12. Sergent N, Lamonier JF, Aboukais A (2000) Chem Mater 12:3830
13. Bensalem A, Verduraz FB, Delamar M, Bugli G (1995) Appl Catal A: Gen 121:81
14. Overbury SH, Huntley DR, Mullins DR, Glavee GN (1998) Catal Lett 51:133
15. De Leitenburg C, Trovarelli A, Zamar F, Maschio S, Dolcetti G, Llorca J (1995) J Chem Soc Chem Commun 2181
16. Mani TV, Varma HK, Damodaran AD, Warrier KGK (1993) Ceram Int 19:125
17. Izu N, Murayama N, Shin W, Matsubara I, Kanzaki S (2004) Jpn J Appl Phys, Part 1 43:6920
18. Bui W, Choy KL, Stelzer NHJ, Scoonman J (1999) J Solid State Ionics 116:225
19. Yoldas BE (1993) J Sol–Gel Sci Technol 1:65
20. Mingos DMP, Baghurst DR (1991) Chem Soc Rev 20:1
21. Fu Y-P, Lin C-H (2003) J Alloys Compds 354:232
22. Reddy BM, Reddy GK, Khan A, Ganesh I (2007) J Mater Sci 42:3557
23. Kiminami RHGA, Morelli MR, Folz DC, Clark DE (2000) Bull Am Ceram Soc 79:63
24. Park S-E, Chang J-S, Hwang YK, Kim DS, Jhung SW, Hwang JS (2004) Catal Surv Asia 8:91
25. Clark DE, Amad I, Dalton RC (1991) Mater Sci Eng A 144:91
26. Kappe CO, Stadler A (2005) Microwave in organic and medicinal chemistry, chapter 2. Wiley–VCH, Weinheim, p 9
27. Sen T, Tiddy GJT, Casci JL, Anderson MW (2003) Angew Chem Int Ed 42:4649
28. Reddy BM, Lakshmanan P, Loridant S, Yamada Y, Kobayashi T, Cartes CL, Rojas TC, Fernandez A (2006) J Phys Chem B 110:9140
29. Reddy BM, Khan A, Lakshmanan P, Aouine M, Loridant S, Volta J-C (2005) J Phys Chem B 109:3355
30. Kenevey K, Valdivieso F, Soustelle M, Pijolat M (2001) Appl Catal B: Environ 2:93
31. Reddy BM, Khan A (2005) Catal Surv Asia 9:155
32. Kozlov AI, Kim DH, Yezerets A, Andersen P, Kung HH, Kung MC (2002) J Catal 209:417
33. Bozo C, Gaillard F, Guilhaume N (2001) Appl Catal A: Gen 220:69
34. Colon G, Pijolat M, Valdivieso F, Vidal H, Kaspar J, Finocchio E, Daturi M, Binet C, Lavalley JC, Baker RT, Bernal S (1998) J Chem Soc Faraday Trans 94:3717
35. Yashima M, Arashi H, Kakihana M, Yoshimura M (1992) J Am Ceram Soc 7:1541
36. Shannon RD (1976) Acta Crystallogr A: Cryst Phys Diffr, Theor Gen Crysallogr 32:751
37. Weckhuysen BM, Schoonheydt RA (1999) Catal Today 49:441
38. Gao X, Wachs IE (2000) J Phys Chem B 104:1261
39. Liu G, Rodriguez JA, Hrbek J, Dvorak J, Peden CHF (2001) J Phys Chem B 105:7762

40. Feigin LA, Svergun DI (1987) Structure analysis of by small angle X-ray and neutron scattering. Plenum Press, New York
41. Liotta LF, Longo A, Macaluso A, Pantaleo G, Venezia AM, Deganello G (2004) Appl Catal B: Environ 48:133
42. Hirata T, Asari E, Kitajima M (1994) J Solid State Chem 110:201
43. Escribano VS, Lopez EF, Panizza M, Resini C, Amores JMG, Busca G (2003) Solid State Sci 5:1369
44. Martinez-Arias A, Fernandez-Garcia M, Arias AM, Garcia MF, Salamanca LN, Valenzuela RX, Conesa JC, Soria J (2000) J Phys Chem B 104:4038
45. Shyu JZ, Weber WH, Gandhi HS (1988) J Phys Chem 92:4964
46. Spanier JE, Robinson RD, Zhang F, Chan S-W, Herman IP (2001) Phys Rev B 64:245407
47. Mc Bride JR, Hass KC, Poindexter BD, Weber WH (1994) J Appl Phys 76:2435
48. Reddy BM, Lakshmanan P, Khan A, Loridant S, Cartes CL, Rojas TC, Fernandez A (2005) J Phys Chem B 109:13545
49. Reddy BM, Lakshmanan P, Bharali P, Sakia P, Thrimurthulu G, Muhler M, Grünert W (2007) J Phys Chem C 111:10478